NANOSCALE BUBBLE STUDY OF CAVITATION INCEPTION ON A PLATINUM SURFACE USING MOLECULAR DYNAMICS SIMULATION

by

Qiang FU, Mengyuan LI, Xiuli WANG*[*]*, Jianen YU, and Rongsheng ZHU

National Research Center of Pumps, Jiangsu University, Zhenjiang, Jiangsu, China

Original scientific paper
https://doi.org/10.2298/TSCI180212019F

The transient properties of liquid argon cavitation nuclei in platinum surface were studied by means of molecular dynamics simulation. The bubble nucleation, with a certain size and stability on the wall surface, was studied by different tensile distances and different wall wettabilities. Also the parameters of cavitation nuclei development, the system pressure, and the total pressure were analysed. The stability of cavitating nucleus growth is closely related to the metastable degree of the system and the wettability of the wall. The tensile distance of the wall surface has a critical value, and stretching greater than the critical value will induce a greater degree of instability in the system, which is conducive to the growth of the cavitation nucleus. A hydrophobic wall is more conducive to the growth of a cavitation nucleus, which is beneficial to spontaneous growth among cavitated nuclei, whereas a hydrophobic exerts has an inhibitory influence on cavitation nuclei.

Key words: *bubble nucleation, molecular dynamics simulation, wettability, hydrophobic, hydrophilic*

Introduction

Cavitation is the process of phase transition in liquids and their vapours occurring in the liquid or on the solid-liquid interface due to hydrodynamic factors: cavitation is unique to liquids, whose essence is phase transition. Cavitation will result in hydraulic performance reduction, erosion material surface, and other hazards, therefore, the early research on cavitation damage has been key to its adoption by industry [1-3], however a great deal of research focuses on the macroscopic phenomenon of cavitation, with the deepening of this research, people gradually realised that nucleation is very important in the process of cavitation, and cavitation nuclei are one of the three factors that influence cavitation [4, 5]. Huang [6] studied the effects of gas composition on cavitation in gas cores and finds that there are different cavitation phenomena prevailing in the gas core.

The nuclear scale is extremely small in cavitation terms, differing from that of the macroscopic bubble, so in recent years, the study of cavitation on a micro-level has become more popular [7-13]. Morch [10, 11] (inter alia) discuss the tensile strength of water and the generation of gas nuclei, then the nucleation phenomena of solid-liquid interface was studied, and the experimental results verified theoretically. Considering the differences between the theoretical and experimental results, Andersen *et al*. [12] and others studied the experimental and theoretical results pertaining to the cavitation interface. The results show that the cavitation nu-

---

[*] Corresponding author, e-mail: 414514657@qq.com

cleation caused by cavitation is smaller than that predicted by theoretical calculation. With the development of gas-core theory and experimental research, the research on gas-core simulation has developed and there are many means of gas-nucleus simulation, and in these simulation methods, due to the advantages of molecular simulations in describing the atomic level, molecular simulation technology has developed into a powerful research tool for scientists in many fields. Many researchers attempt to use molecular simulation study nucleation phenomenon. For research into homogeneous nucleation: Kinjo and Matsumoto [14], Yasuoka and Matsumoto [15], and Wu and Chin [16] stretched the Lennard-Jones fluid system, to impose a negative pressure on the system, and the homogeneous bubble nucleation process in homogeneous fluids was studied. According to the simulation results, when the system is pulled to a certain degree and the density of the system is low, the system will develop stable bubbles. For the study of heterogeneous nucleation: Shinichi *et al*. [17] compared the differences in cavitation nucleation and homogeneous nucleation under the presence of heterogeneous atoms in a Lennard-Jones fluid, and it was found that the gas nuclei merged in the process of the single-phase liquid nucleation more frequently, while the gas nuclei are rarely merged during the liquid nucleation of heterogeneous atoms, and was stable in the vicinity of heterogeneous atoms.

Although the molecular simulation of fluid internal cavitation has been long-studied, no consideration has been given to the effect of the solid-liquid interface on cavitation, so more researchers now use molecular simulation study the microscopic effects of liquid on the solid-liquid boundary. Schoen *et al*. [18] used molecular dynamics simulations to study the phase transition of a simple liquid defined between two parallel walls at intervals of several millimetres. In addition the simple phase change observation of cavitation, Maruyama and Kimura [19] used molecular dynamics to simulate the heterogeneous nucleation of bubbles on a solid surface in a nanochannel. Liquid Ar is placed between the parallel solid surfaces, and the simulated region is pulled up until nucleation occurs. On the question of how to establish a connection between micro-cavitation and macro-cavitation, Nagayama *et al.* [20] used molecular dynamics simulations to simulate and observe the changes in nanoscale bubbles under different solid-liquid interfacial wettability conditions for metastable liquids in nanosized channels under an applied inlet force. It was also found that the vapour pressure inside the nanobubbles is inconsistent with the macroscopic Laplace equation.

As aforementioned, the molecular simulation of the cavitation nucleus has been developed to some extent, including the molecular simulation of homogeneous nucleation, heterogeneous nucleation, and the solid-liquid interface, but there are still many microscopic factors affecting the growth of cavitation nucleus. Therefore, in this paper, the influences of different tensile strengths of solid wall and wall wettability on the cavitation nuclei have been simulated.

Simulation model

In this paper, Lammps software is selected as the molecular dynamics (MD) simulation software: as shown in fig. 1(a), the entire simulation region is set to 100 Å (x) × 100 Å (y) × 120 Å (z), and periodic boundary conditions are used in the x- and y-directions. The top and bottom of the simulation area are Pt atom walls measuring 100 Å (x) × 100 Å (y) × 8 Å (z). The Pt atoms are set as fixed atoms and the initial position is arranged by the FCC dense-row cubic lattice distribution, and the atomic mass of Pt is 195.09 g/mole and the number of atoms is 10000. The Ar atom simulation field is arranged in the middle region of the upper and lower Pt atom simulation layer and the number of atoms is 17000, and the atomic mass of Ar is 39.948 g/mole. The simulation domain size is 100 Å (x) × 100 Å (y) × 104 Å (z), and the initial position arrangement adopts an FCC dense row cubic lattice distribution. The cut-off radius used in this paper is the spherical truncated radius of $4\sigma_{\text{Ar-Ar}}$, with a time step of 0.5 fs. After confirm that the initial cavitation radius in the simulated region was 30 Å, atoms inside the bubble nucleus were deleted. The cavitation nuclei stability can be changed by extension of the wall and a cavitation nucleus with a 30 Å radius is selected.

Here, the time integration is done with velocity Verlet algorithm, and the simulation process is divided into three parts. The first part is a relaxation process, in the absence of solid-liquid interaction, the system temperature is stabilised at 85 K, running for 1000 steps. After the system is stabilised, a cavitation nucleus with a radius of 30 Å is excavated centred at 50 Å (x) × 50 Å (y) × 60 Å (z), and the z-direction of the simulated domain is stretched to simulate tension, the velocity of this stretch is set to 2.5 Å/fs, 5 Å/fs, and 12 Å/fs. After stretching, the system runs for 10000 steps in this condition. In the data output phase, the data are output once every 100 steps.

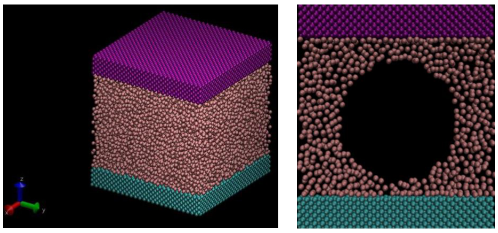

Figure 1. The model

Here, the primary cavitation of solid surface is studied by molecular simulation. Using the L-J (12-6) fluid potential function, the specific form:

$$\phi(r) = 4\varepsilon\left[\left(\frac{\sigma}{r}\right)^{12} - \left(\frac{\sigma}{r}\right)^{6}\right] \tag{1}$$

where r is the distance between molecules, Φ – the energy, ε – the potential well depth, and σ – the characteristic length. For hydrophilic Pt wall surfaces, $\varepsilon_{\text{Ar-Ar}} < \varepsilon_{\text{Ar-Pt}}$. The L-J potential parameters of Ar-Ar and Ar-Pt used in this paper are: $\sigma_{\text{Ar-Ar}}$ = 3.405 Å, $\varepsilon_{\text{Ar-Ar}}$ = 0.01032 eV, $\sigma_{\text{Pt-Pt}}$ = 2.475 Å, $\varepsilon_{\text{Pt-Pt}}$ = 0.676 eV, $\sigma_{\text{Ar-Pt}}$ = 2.94 Å. For hydrophilic Pt wall surfaces, $\varepsilon_{\text{Ar-Ar}} < \varepsilon_{\text{Ar-Pt}}$ ($\varepsilon_{\text{Ar-Pt}}$ has a value of 0.083 eV). For hydrophobic Pt wall surfaces, $\varepsilon_{\text{Ar-Ar}} > \varepsilon_{\text{Ar-Pt}}$ (the value of $\varepsilon_{\text{Ar-Pt}}$ is 0.00215 eV).

Simulation results and analysis of wall cavitation nucleation under different tensions

Here, the upper and lower walls are all set to the hydrophilic wall (the value of $\varepsilon_{\text{Ar-Pt}}$ is 0.083 eV). The initial centre of the cavitation nucleus is located at 50 Å (x) × 50 Å (y) × 60 Å (z) in the simulation region, and the initial dimension of the cavitation core is 30 Å. To obtain the growth status of the cavitating nucleus under different tensions, energy minimisation and relaxation treatment of the calculation domain were undertaken before stretching the system.

Evolution process of wall cavitation nucleation

To visualise the evolution of the cavitation nuclei under different wall strains, we adopted the diagram shown in fig. 2, to select the slice charts at 75 ps and 150 ps, respectively.

It can be seen from the evolution process of the cavitation nuclei shown in fig. 2 that there are similarities and difference over time under the different stretching distances applied to the upper wall. The 75 ps slice chart shows that when the upper wall is stretched to 0.25 nm, the cavitation nuclei are slightly elongated along the z-direction, and the overall form is micro-elliptic. When the upper wall stretching distance of the system is 0.5 nm, the cavitation nucleus is also observed to be elliptical in the 75 ps slice graph, but the long axis of the ellipse becomes even longer. When the upper wall is stretched by a distance of 1.2 nm, the formation of cavitation nuclei

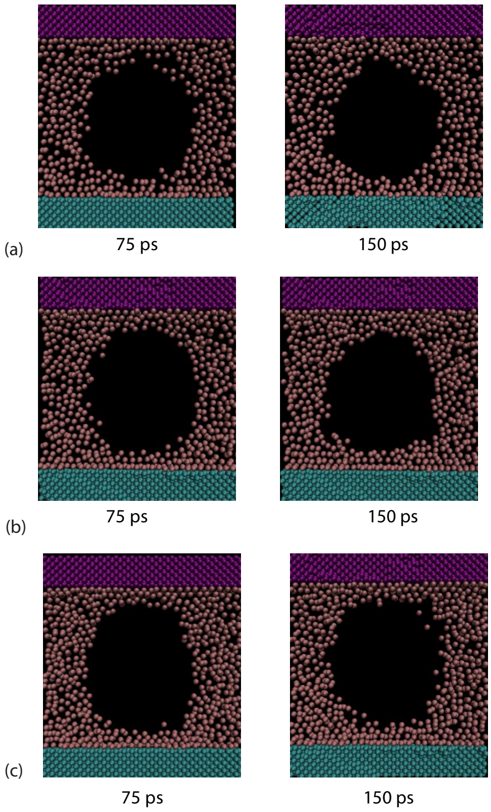

Figure 2. Slice diagram of evolution process of cavitation nucleus; (a) upper wall stretch 0.25 nm, (b) upper wall stretch 0.5 nm, and (c) upper wall stretch 1.2 nm

Table 1. The variables of cavitation bubble

Stretching distance [nm]	Ellipse long axis [Å]	Volume increase, ΔV [nm^3]
0.25	62	0.3
0.5	64	1.8
1.2	68	6.44

in the growth process is seen to be proportional to the degree of instability of the system. When the system is subjected to the tensile force generated by the negative pressure, and the direction of the resulting tensile force is in the z-direction, the cavitation nucleus is deformed along the z-axis by this tensile force. As the stretching distance increases, the decrease in the external pressure on the cavitation nucleus increases, the tensile force associated with the cavitation nucleus increases, and the deformation of the cavitation nucleus also becomes larger. The aforementioned elliptical long axis can clearly describe the shape difference, which coincides with the phenomenon whereby the force shape of the bubble undergoes a macroscopic change. The variables of cavitation bubble was shown in the tab. 1.

With the further growth of the cavitation nucleus, as shown in the 150 ps slice diagram, when the upper wall stretching distance of the system is 0.25 nm, the shape of the cavitation core reverts to a circle, and the volume basically remains unchanged. When the upper wall is stretched by a distance of 0.5 nm, the volume of the cavitating nucleus increases slightly after the circle is restored. When the upper wall is stretched by 1.2 nm, the volume of the cavitation nucleus increases obviously after the circular recovery: this shows that the growth of cavitation nuclei is related to the degree of instability in the system pressure, as the size of the initial cavitation nucleus used in the simulation are the same, excluding the effect of the dimensions of cavitation nuclei. When the system is influenced by negative pressure, the tensile force equals the interatomic interaction force between Ar atoms, and the volume of the cavitation nuclei will not change significantly. When the tensile force generated by negative pressure is greater than the interatomic interaction force between Ar atoms, the volume of the cavitating nucleus increases. With the increase of the system extension, the instability of system pressure increases, and the volume change in the cavitation nucleus also increases.

Atomic density distribution in the z-direction for the growth of cavitation nuclei in the wall

For a more intuitive observation of the growth of the cavitation nucleus, fig. 3 shows the z-direction density distribution curves of the Ar atoms with different tensile degrees under the hydrophilic wall conditions, at stretching distances of 0.25 nm, 0.5 nm, and 1.2 nm,

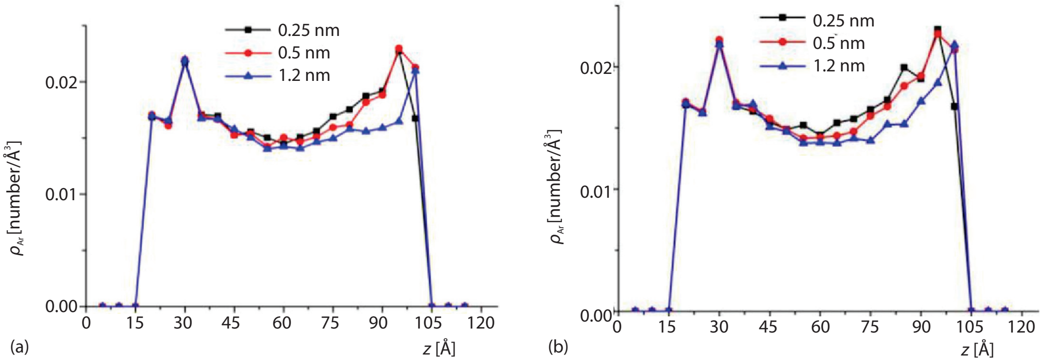

Figure 3. Density distribution curve of Ar atoms in the z-direction under different tensile strains between hydrophilic middle wall surfaces; (a) 75 ps, (b) 150 ps

respectively. Figure 3(a) shows the *z*-direction density curve after a simulation time of 75 ps: the three stretching distance are all in the *z*-direction and are between 15 Å and 30 Å and the density of Ar atoms increased. The region is close to the lower wall, and the density gradient was caused by the hydrophilic effect of the Ar atoms on the wall surface. A large amount of Ar atoms accumulate on the lower wall, causing the density of Ar atoms to increase in that region. The reasons for the density gradient appearing between 95 Å and 105 Å in the *z*-direction in the same stretching distance between 0.25 nm and 0.5 nm are the same. When the stretching distance is 1.2 nm, this region is between 100 Å and 105 Å long in the *z*-direction, so the larger the stretching distance, the greater the deformation of the cavitation nucleus. In the *z*-direction, at 30 Å and 35 Å, the density of Ar atoms presents a gradient change opposite to that seen previously: this is because the further from the accumulation of wall surface atoms, the greater the interatomic force on the Ar atoms is manifested as a repulsion, so the number of atoms decreases with increasing distance. The reasons for the density gradient appearing between 90 Å and 95 Å in the *z*-direction, over the same stretching distance between 0.25 nm and 0.5 nm, are the same. When the stretching distance is 1.2 nm, this region is between 95 Å and 100 Å in the *z*-direction. The dimension in the *z*-direction of the cavitation nuclei is approximately 55 Å (between 35 Å and 90 Å in the *z*-direction) at a stretching distance of 0.25 nm and 0.5 nm, and the value is 65 Å (between 35 Å and 100 Å in the *z*-direction) when the extension is 1.2 nm. For the three stretching distances analysed here, the minimum density of the Ar atoms in the cavitation nucleus region decreases in turn, showing that the volume of the cavitation nuclei increases with increasing extension.

Figure 3(b) shows the *z*-direction density curve for a simulation time of 150 ps. The same density gradients as seen at 75 ps appear in the area near the wall, but the density is larger in all three cases when close to the upper wall. The result shows that, when the number of stacked atoms on the upper wall surface at 150 ps is greater than that at 75 ps, with the increase of the number of Ar atoms in the wall, atomic stacking extrusion causes the deformation of the cavitation nuclei to recover in the *z*-direction, which is consistent with the phenomenon described in fig. 2. Under three different stretching distances, the average Ar atom density in the 0.25 nm cavitation nucleus region is the same as that at 75 ps, while the average density of Ar atoms in the 0.5 nm and 1.2 nm cavitation nucleus region is smaller than that at 75 ps, indicating that the volume of cavitation nuclei did not increase when stretched by 0.25 nm. The volume of cavitation nuclei at distances of 0.5 nm and 1.2 nm increases markedly, which also coincides with the phenomena described in fig. 2.

In summary, the effects of different stretching distances on the cavitation nuclei existing in the two wall surfaces are different. As the tensile distance increases, the deformation of cavitation nucleus increases. When the deformation of the cavitation nucleus reaches its limit, the cavitation nucleus is restored from an elliptical form to a stable circle due to the surface tension. During the recovery phase, the volume of the cavitating nucleus increases only when the stretching distance exceeds a critical value, and the volume of the cavitation nucleus increases with the increasing distance.

System pressure and energy change

Figure 4(a) shows the system internal pressure variation curve during the cavitation nucleus growth stage. Three lines represent three different stretching distances, and it can be seen that the three curves show the same trend, because the simulation uses a deleted atom to balance the system for a very short period of time, all three curves have a steep drop in the negative pressure applied during the first 8 ps. Although the initial pressure varies with different stretching distances, they are all under a very low negative pressure at which the cavitating nucleus is able to grow and then the system pressure is gradually stabilised. It can be seen from the figure that the final average equilibrium pressure of the system increases with increasing extension.

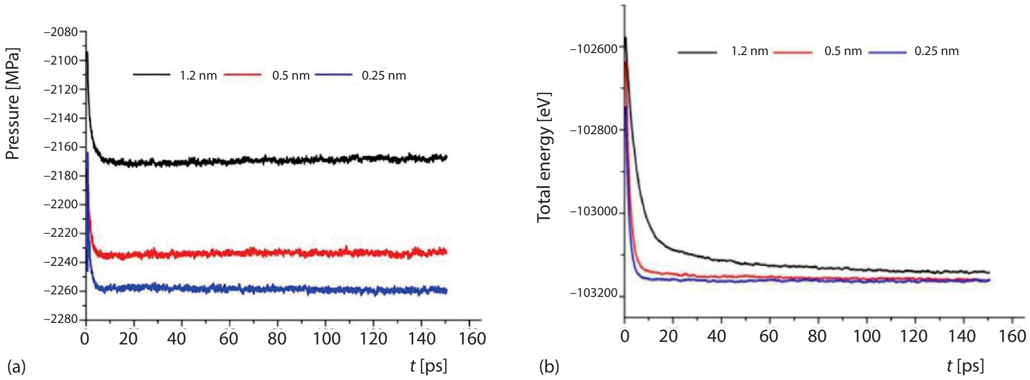

Figure 4. The pressure; (a) and total energy, (b) variation during cavitation nuclear growth

Figure 4(b) shows the total energy variation curve of the system during the hollow growth stage under three different extensions and it can be seen that the system total energy change trend is the same during application of three different stretching distances, but the time required to balance the system energy is longer than the time taken to extend it by 0.5 nm and 0.25 nm when the overall stretching distance is 1.2 nm. As the stretching distance increases, the metastability of the system is more impaired, so the energy of the system is unchanged after the system is finally stabilised at 0.25 nm. The energy of the system is decreased slightly when the system is stable at 0.5 nm, and the energy decrease at 1.2 nm is more obvious. This is because there is no change in the size of cavitation nuclei at 0.25 nm so there is no energy absorbed thereby. At 0.5 nm and 1.2 nm, the dimension of the cavitation nuclei increases gradually, and their growth process is a spontaneous process with a reduced free energy, so the total energy of the system gradually decreases. The change in the size of the cavitation nucleus is the largest, therefore, the system's tendency to decrease in energy is more obvious.

So from the perspective of energy changes can be drawn, when the initial cavitation nucleus is constant, the greater the wall stretching distance, the more unstable the system and the more vigorous the cavitation that occurs.

Simulation results and analysis of cavitation nucleation variations for different wall wetting degrees

In this chapter, two types of wettability wall conditions are set: one is such that the upper and lower wall surface are set to be hydrophilic ($\varepsilon_{\text{Ar-Pt}}$ is 0.083 eV), and the other is such that the upper and lower wall are set to be hydrophobic ($\varepsilon_{\text{Ar-Pt}}$ is 0.00215 eV).

The evolution of hydrophilic and hydrophobic wall cavitation nucleation

This chapter simulates the 75 ps and 150 ps slices of the hydrophilic, and hydrophobic, walls when the tensile wall extension is 1.2 nm.

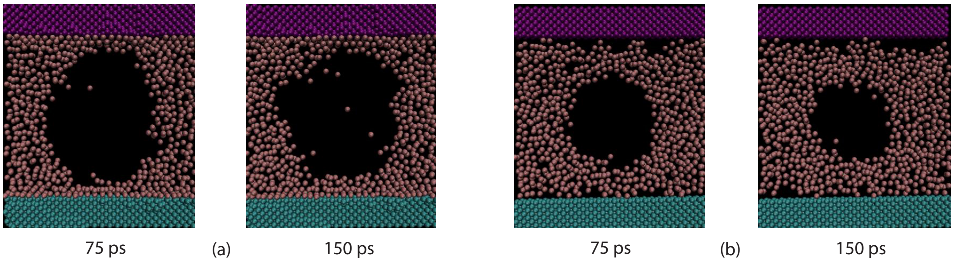

Figure 5. Slice diagram showing evolution of a cavitation nucleus; (a) hydrophilic wall, (b) hydrophobic wall

From the evolution process of the cavitation nucleus shown in fig. 5, it can be seen that the evolution process of the cavitation nucleus differs over time. As shown in fig. 5(a), the upper and lower wall surfaces of the system were set to be hydrophilic, and over time, the shape of the cavitation nucleus changed from circular to oval, and then backed to circular. The final volume had increased. Figure 5(b) shows that, when the upper and lower wall surfaces of the system were set be to hydrophobic, there was no obvious change in the shape of cavitation nucleus, but the volume decreased. Over time, a cavity appeared near the wall at 75 ps. At 150 ps, the volume of the cavity increased significantly. Hydrophilic wall atoms, due to the hydrophilic effect, they gradually gathered over the wall surface and atoms on both sides of the cavitation nucleus accumulate on both sides of the upper and lower walls. As the number of stacked atoms increases, some of the atoms stacked on both sides of the wall are squeezed toward the top of the cavitating nucleus, and the compressed atoms force the cavitation nucleus downwards, because the atoms accumulate on the upper and lower walls, the atomic density of the central part is reduced so as to facilitate the development of the cavitation nucleus, so the cavitation nucleus becomes circular having originally been elliptical. As the hydrophobic wall atoms are affected by hydrophobicity, the atoms on the wall gradually gather in the middle region of the upper and lower walls. As the number of aggregated atoms increases, the distance between the atoms decreases, the interaction between the molecules is enhanced and the tensile force is greater than that in the system affected by the negative pressure, and the volume of the cavitated nucleus decreases. The variables of cavitation bubble was shown in the tab. 2.

Table 2. The variables of cavitation bubble

Wettability	Hydrophilic	Hydrophobic
Volume change, ΔV [nm^3]	6.44	–11.078

Atomic density distribution in the z-direction on the hydrophilic and hydrophobic wall surface

To observe the effect of wall wettability on the growth of cavitation nuclei, fig. 6 depicts the density distribution of Ar atoms in the z-direction in the middle of the wall when the upper and lower walls are set to be hydrophilic and hydrophobic, respectively. As shown in fig. 6(a), at 75 ps, the density of Ar atoms above the hydrophilic wall sharply increases and then drops steeply between 15 Å and 30 Å in the z-direction. This is because the hydrophilic wall is conducive to the adsorption of Ar atoms, and the Ar atoms accumulate on the top of the wall so that the initial number density increases. With the increase of z-distance, the interatomic force plays a leading role so that the atomic density decreases as shown in the figure, however, due to the hydrophobicity of the hydrophobic wall surface, the phenomenon of atomic packing on the wall surface did not occur, so the number density of Ar atoms does not exhibit the aforementioned change. At z = 15 Å, the density of the Ar atoms on the hydrophobic wall is much less than that on the hydrophilic wall. It is shown that the part of hydrophobic wall close to the wall is affected by hydrophobicity and a large number of atoms are far from the wall, which is consistent with the phenomenon described in fig. 5. The variation in the density of Ar atoms on the two wetting upper wall surfaces is the same as that of the lower wall, and the reason for this is the same. In the case of hydrophilic, and hydrophobic, walls, the average density of Ar atoms in the cavitation nucleus region of the hydrophilic wall is greater than that of a hydrophobic wall. The size of the cavitation nucleus is 6 Å and 5 Å, respectively, because the hydrophilic wall Ar atoms accumulate on the upper and lower wall surface, the central simulation region of the local Ar atom density is low, and thus conducive to the growth of cavitation nuclei. However, the hydrophobic surface of the Ar atoms move toward the central region, which causes the cavitation nuclei in the central region be squeezed by the Ar atoms moving up and down to cause a decrease in volume. This shows that the volume of the hydrophobic wall cavitation nucleation is smaller than that with a hydrophilic wall under the same extension, which is consistent with the phenomenon described in fig. 5.

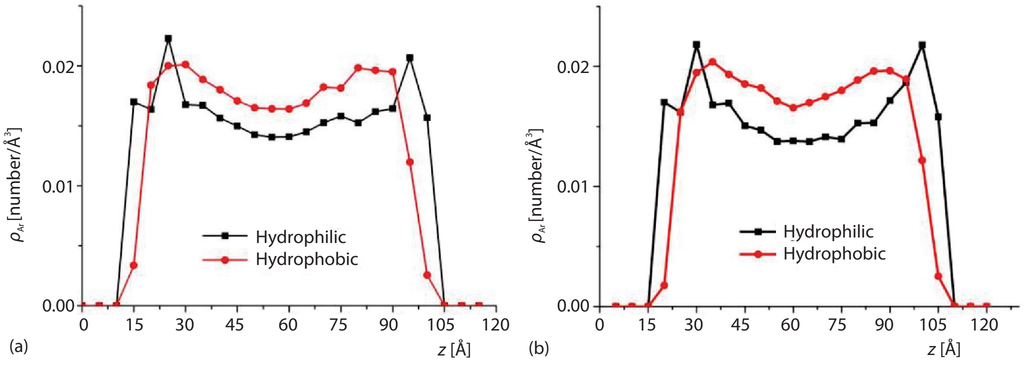

Figure 6. Density distribution curve of Ar atoms between the hydrophilic, and hydrophobic, wall surfaces in the z-direction; (a) 75 ps, (b) 150 ps

At 150 ps as shown in fig. 6(b), at 15 Å in the *z*-direction, the density of the Ar atoms above the hydrophobic lower wall is significantly lower than that at 75 ps (from 0.0038 to 0.0023), indicating that the number of Ar atoms on the lower wall surface is reduced. Similarly, the density of Ar atoms on the upper wall at 100 Å is also decreased (from 0.0027 to 0.0025). That is, more Ar atoms escape from the two walls while the number of Ar atoms near the hydrophilic wall does not change. At this time, the average size of the hydrophobic wall cavitation nucleus is 2 Å smaller than that at 75 ps, which is about 15 Å smaller than that under hydrophilic wall cavitation conditions in the same period, which is in accordance with the data in fig. 5.

System pressure and energy changes

Figure 7(a) shows the internal pressure variation curve of the system during the cavitation nucleus growth stage under different wall wettabilities. The two lines represent the hydrophilic wall and hydrophobic wall, respectively, and it can be seen that under the extension, the two curves show the same trend, but the initial pressure is different because of the different wettability, because of the extremely low negative pressure, the hydrophilic wall creates a good growth environment for the cavitation nuclei, so the size of the cavitation nuclei increases. Although the hydrophobic wall is also under a negative pressure (800 MPa) greater than that acting in the case of a hydrophilic wall, it is not conducive to the growth of cavitation nuclei. Therefore, it can be concluded that the hydrophilic wall is conducive to the growth of cavitation nuclei, and hydrophobic walls inhibit the growth of cavitation nucleus.

Figure 7. The pressure; (a) and total energy, (b) variation curve in the cavitation nuclear growth phase

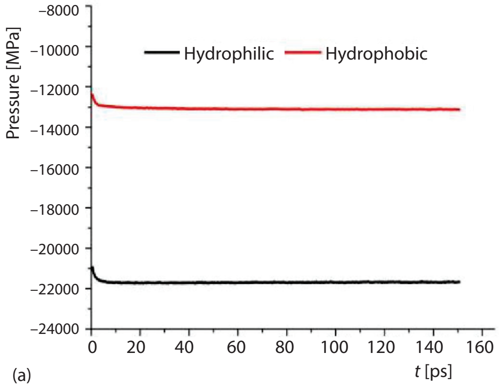

(a)

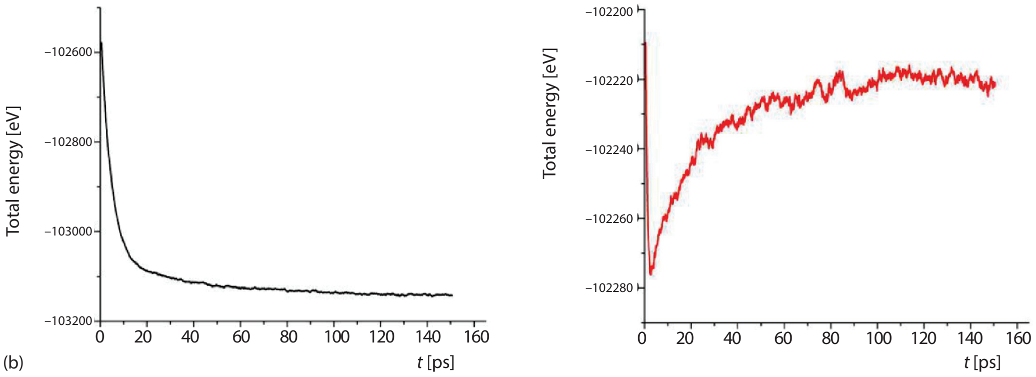

(b)

Figure 7(b) shows the total energy variation of the system during the cavitation nuclear growth phase under different wall wettabilities. Under the same extension and initial cavitation nucleus size, the total energy of the system varies significantly during the different wall wettability stages of cavitation nucleation. In the case of a hydrophilic wall, the system energy is gradually reduced due to the increase of the cavitation nucleus dimension caused by the metastable state. Whereas the hydrophobic wall exhibits the opposite behaviour because the cavitating nucleus of the hydrophobic wall is reduced in size by atomic squeezing, and the increase of the interatomic potential energy causes the system pressure to be continuously increased.

So from the perspective of energy change, when the initial cavitation nucleus and tensile strain are constant, the stronger the hydrophilicity, the more vigorous the cavitation that occurs: the stronger the hydrophobicity, the smaller the cavitation nuclei.

Conclusions

The molecular dynamics simulation method is used to analyse the growth of stable cavitation nuclei in the liquid Ar between two Pt walls under different stretching distances and different wall wettabilities. The following conclusions are drawn:

When there are stable cavitation nuclei with the same volume in liquid Ar, the tensile strain in the upper wall has a critical value and some critical metastable state. When the stretching distance is less than this critical value, the volume of the cavitation nucleus in the liquid Ar remains unchanged or decreases. When the extension exceeds this critical value, the volume of the cavitation nucleus increases: it is indicated that there is a critical metastable state in the cavitation nuclei of the same dimension, and only when reaching this critical metastability can it be conducive to the development of cavitation. Under the same size of cavitated nuclei and the same extension, the volume of cavitation nuclei on the hydrophilic wall surface increases and the volume of cavitating nuclei on the hydrophobic wall surface decreases. The energy of the hydrophobic wall system gradually increases and that in the system with a hydrophilic wall gradually decreases, *i. e.*, the hydrophilic wall is more conducive to the development of cavitation than the hydrophobic wall surface.

References

[1] Guan, X. F., *Modern Pumps Theory and Design*, China Astronautic Publishing House, Beijing, China, 1995

[2] Pan, S. S., *China Encyclopedia (Mechanics volume)*, “Cavitation” Article, Encyclopedia of China Publishing House, Beijing, China, 1985

[3] Yuan, D. Q., *et al*., Research Progress of Cavitation and Erosion in Hydraulicm Achinery, *Drainage and Irrigation Machinery*, *27* (2009), 4, pp. 269-272

[4] Hidalgo, V., *et al*., Numerical Simulation of Cavitating Flow over 2d Hydrofoil Using Openfoam Adapted for Debian Operating System with Lxde Based in Kernel Gnu/linux, *Proceedings*, ASME 4th Joint Us-european Fluids Engineering Division Summer Meeting and International Conference on Nanochannels, Chikago, Ill., USA, 2014

[5] Cervone, A., *et al*., Thermal Cavitation Experiments on a Naca0015 Hydrofoil, *Journal of Fluids Engineering*, *128* (2006), 2, pp. 326-331

[6] Huang, J. Q., Composition of Gas Nucleus and Its Influences on Cavitation, *Chinese Journal of Hydrodynamics*, (1992), 2, pp. 138-140

[7] Blander, M., Bubble Nucleation in Liquid, *Advances in Colloid and Interface Science*, *10* (1979), 1, pp. 1-32

[8] Gindroz, B., Cavitation Nuclei and Cavitation Inception of Marine Propellers: State of the Art at the Dawn of the of the 21st Century, *JSME International Journal*, *41* (1998), 2, pp. 464-471

[9] Tanaka, K. K. Tanaka, H., Simple Improvements to Classical Bubble Nucleation Models, Phys. Rev. E Stat. Non-Lin. Soft Matter Phys., *92* (2015), 2, 022401

[10] Morch., K. A., Cavitation Nuclei: Experiments and Theory, *Hydrodynamics*, *21* (2009), 2, pp. 176-189
[11] Morch, K. A., Cavitation Inception from Bubble Nuclei, *The Royal Society*, 5 (2015), 2, pp. 1-13
[12] Andersen, A., *et al*., Cavitation Nuclei in Water Exposed to Transient Pressures, *Journal of Fluid Mechanics*, *771* (2015), May, pp. 424-448
[13] Bapat, P. S., Pandit, A. B., Thermodynamic and Kinetic Considerations of Nucleation and Stabilization of Acoustic Cavitation Bubbles in Water, *Ultrasonics Sonochemistry*, *15* (2008), 1, pp. 65-77
[14] Kinjo, T., Matsumoto, M., Cavitation Processes and Negative Pressure, *Fluid Phase Equilibria*, *144* (1998), 1-2, pp. 343-350
[15] Yasuoka, K., Matsumoto M., Molecular Dynamics of Homogeneous Nucleation in the Vapor Phase, Lennard-Jones Fluid, *Journal of Chemical Physics*, *109* (1998), 19, pp. 8451-846
[16] Wu, Y. W., Chin, P., A Molecular Dynamics Simulation of Bubble Nucleation in Homogeneous Liquid under Heating with Constant Mean Negative Pressure, *Nanoscale and Microscale Thermophysical Engineering*, *7* (2003), 2, pp.137-151
[17] Shinichi, T., *et al*., A Study on the Growth of Cavitation Bubble Nuclei Using Large-Scale Molecular Dynamics Simulations, *Fluid Dynamics Research*, *40* (2008), 7-8, pp. 606-615
[18] Schoen, P. A. E., *et al.*, Phase Change of a Confined Subcooled Simple Liquid in a Nanoscale Cavity, *Physical Review E Statistical Non-Linear and Soft Matter Physics, 71* (2005), 1, 041602
[19] Maruyama, S., Kimura T., A Molecular Dynamics Simulation of Bubble Nucleation on Solid Surface, *Nihon Kikai Gakkai Ronbunshu B Hen/Transactions of the Japan Society of Mechanical Engineers Part B*, *65* (1999), 638, pp. 3461-3467
[20] Nagayama, G., *et al.*, Molecular Dynamics Simulation on Bubble Formation in a Nanochannel, *International Journal of Heat and Mass Transfer*, *49* (2006), 23-24, pp. 4437-4443

Paper submitted: February 12, 2018
Paper revised: January 3, 2019
Paper accepted: January 9, 2019